PHYSICAL REVIEW D **95,** 123009 (2017)

Roadmap for searching cosmic rays correlated with the extraterrestrial neutrinos seen at IceCube

J. A. Carpio and A. M. Gago

Sección Física, Departamento de Ciencias, Pontificia Universidad Católica del Perú, Apartado 1761, Lima, Perú

(Received 10 January 2017; published 16 June 2017)

We have built sky maps showing the expected arrival directions of 120 EeV ultrahigh-energy cosmic rays (UHECRs) directionally correlated with the latest astrophysical neutrino tracks observed at IceCube, including the four-year high-energy starting events (HESEs) and the two-year northern tracks, taken as point sources. We have considered contributions to UHECR deflections from the Galactic and the extragalactic magnetic field and a UHECR composition compatible with the current expectations. We have used the Jansson-Farrar JF12 model for the Galactic magnetic field and an extragalactic magnetic field strength of 1 nG and coherence length of 1 Mpc. We observe that the regions outside of the Galactic plane are more strongly correlated with the neutrino tracks than those adjacent to or in it, where IceCube HESE events 37 and 47 are good candidates to search for excesses, or anisotropies, in the UHECR flux. On the other hand, clustered northern tracks around $(l, b) = (0°, -30°)$ and $(l, b) = (-150°, -30°)$ are promising candidates for a stacked point source search. For example, we have focused on the region of UHECR arrival directions, at 150 EeV, correlated with IceCube HESE event 37 located at $(l, b) = (-137.1°, 65.8°)$ in the northern hemisphere, far away from the Galactic plane, obtaining an angular size $\sim 5°$, being $\sim 3°$ for 200 EeV and $\sim 8°$ for 120 EeV. We report a p value of 0.20 for a stacked point source search using current Auger and Telescope Array data, consistent with current results from both collaborations. Using Telescope Array data alone, we found a projected live time of 72 years to find correlations, but clearly this must improve with the planned Auger upgrade.

DOI: 10.1103/PhysRevD.95.123009

I. INTRODUCTION

The discovery of extraterrestrial neutrinos made by the IceCube (IC) Neutrino Observatory [1–3] has boosted the multimessenger searches of point sources, the eventual results of which should lead us to understanding the high-energy astrophysical phenomena. Within this context, it is believed that extraterrestrial neutrinos are created inside or outside the source, primarily through photopion production. The pion production is caused by the interaction of ultrahigh-energy cosmic rays (UHECR) either with the cosmic microwave background (CMB) or with the extragalactic background light [4], yielding neutrinos from their decay, with energies in the range of 10 PeV–1 EeV or in $\mathcal{O}(\mathrm{PeV})$, respectively. Thus, given the connection between UHECRs and neutrinos, some degree of correlation between their respective experimental observations is expected. This kind of study has been already conducted using the extraterrestrial neutrinos observed at IceCube and combined UHECR data from the Pierre Auger Observatory (PAO) and Telescope Array (TA), with no positive outcome yet [5]. There have also been other attempts to seek correlations between photons and neutrinos [6] or gravitational waves with neutrinos [7]. In the future, multimessenger searches, such as joint neutrino/gamma-ray transient sources, will be facilitated by AMON [8].

The correlation analysis between UHECRs and neutrinos, as has been done in Ref. [5], relies on the distribution of cosmic-ray arrival directions. This paper uses another approach to this issue. In our case, we will focus on predicting the regions on the sky where UHECRs correlated with neutrinos are expected to arrive, considering that the neutrino tracks are pointing to the sources. In this way, these regions will constitute a tool for searching UHECR excesses on the sky. Besides, searches in these regions could be used as complementary test of the various hypotheses implied in their construction: among others, the magnetic field model; the UHECR composition; and, at a more fundamental level, the expected associated production of UHECRs and neutrinos.

In fact, the choice of the Galactic and extragalactic magnetic field model is one of the most important hypotheses in our work. These fields deviate the UHECRs from their path to the Earth, making their arrival directions not coincide with the corresponding ones of the neutrinos. For the extragalactic magnetic field (EGMF), we will use a turbulent field of strengths ~ 1 nG and coherence lengths $\gtrsim 1$ Mpc following Refs. [9,10]. For the Galactic magnetic field (GMF), we will use field strengths of ~ 1 μG. The GMF is divided into a regular and a turbulent component, the former described by models such as those in Refs. [11,12] and the latter described in Ref. [13]. The

GMF deflections are dominated by the regular components, to which is added, as a secondary effect, a smearing due to the turbulent component. Another premise in the calculation of the magnetic deviation is the UHECR mass composition, which is taken into account in this paper, as it is described in the sections ahead. Currently, the PAO has yet to explore the mass composition above 50 EeV, although a trend toward a heavy composition above 10 EeV is apparent [14,15]. We select 13 muon tracks from the extraterrestrial neutrino data sample given by IceCube in the 79-string and 86-string configurations [1–3], which spans the deposited energy range 60 TeV–1 PeV. This is equivalent to four years of data taking and gives us an $E_\nu^{-2.58}$ neutrino flux spectrum and a flux of $2.2 \pm 0.7 \times 10^{-18}$ GeV^{-1} cm^{-2} s^{-1} sr^{-1} at 100 TeV. We choose 21 muon neutrino tracks from the two-year sample [16], consisting of tracks coming from the northern hemisphere, containing approximately 35,000 muon tracks.

It is important to remark that the energies of IceCube neutrinos are not energetically correlated to those of the UHECR detected by PAO and TA. However, it does not exclude the possibility that the UHECR and IC neutrinos came from the same source, since these sources can produce lower-energy cosmic rays which are compatible with the IC neutrinos. It is also viable that the neutrino sources cannot accelerate cosmic rays to ultrahigh energies, in which case we would see no correlation at all.

The paper is divided as follows. In Sec. II, we describe the analysis ingredients, which are the extragalactic magnetic field deflections with their corresponding treatment for UHECR propagation, the Galactic magnetic field deflection, and the definitions for signal and background. In Sec. III, we present our results, and, finally, in Sec. IV, we present our conclusions.

II. ANALYSIS INGREDIENTS

We divided this section into three subparts: the EGMF deflections and UHECR propagation, GMF deflections, and the signal and background definitions.

A. EGMF deflections and UHECR propagation

Typical deflections in a turbulent EGMF with a Kolmogorov spectrum are given by [10]

$$\delta_{\rm rms} = 0.8^\circ Z \left(\frac{B_0}{E}\frac{10^{20}\ {\rm eV}}{10^{-9}\ {\rm G}}\right)\sqrt{\frac{D}{10\ {\rm Mpc}}}\sqrt{\frac{L_c}{1\ {\rm Mpc}}}, \quad (1)$$

where B_0 is the EGMF root-mean-square field strength, E is the UHECR energy, L_c is the coherence length of the field, and D is the propagation distance, which starts from the UHECR. There is no general consensus on the values of B_0 and L_c [9,10]; in particular, we are using the values of 1 nG and 1 Mpc, respectively. Because of the large propagation distances of order >10 Mpc, energy losses are taken into account, being obtained from forward tracking via Monte Carlo simulation using CRPropa3 [17]. These energy loss processes include cosmological expansion, photopion production, and photodisintegration. For evaluating the losses due to photopion production and photodisintegration, we use the CMB and the infrared background light described in Ref. [18].

We estimate the magnetic deflections through the injection of individual events from the spectrum [19]

$$Q_Z(E_p) \propto \frac{E_p^{-\gamma}}{\cosh[E_p/(ZR_{\rm max})]}, \quad (2)$$

where E_p stands for primary UHECR energy and $R_{\rm max} = 20$ EV marks the rigidity cutoff, where rigidity is defined, in general, as $R = E/(Ze)$. The sources emit p, He, N, Si, and Fe nuclei [19] according to the ratios

$$\mathrm{p:He:N:Si:Fe} = 0.1:0.27:0.30:0.32:0.005, \quad (3)$$

and we assume a homogenous distribution of identical sources. The composition in Eq. (3) fits the Auger data reasonably well and gives us a maximum distance of $\sim$200 Mpc from which UHECR above 100 EeV may reach the Earth. The propagation distance D decreases exponentially with the UHECR arrival energy E.

We then generate 10^6 Monte Carlo events, calculating the magnetic deflection with Eq. (1) for small steps ΔL, due to the energy losses, adding them in quadrature. This amounts to the substitution

$$\frac{Z}{E}\sqrt{D} \to \sqrt{\sum_{i=1}^{N}\frac{Z^2(L)}{E^2(L)}\Delta L}, \quad (4)$$

where $N\Delta L = D$. These magnetic deflections also increase the UHECR propagation length by $\Delta D = \sum_{i=1}^{N}\Delta r$ where

$$\Delta r \simeq 0.195\ {\rm Mpc}\frac{Z^2}{(E/{\rm EeV})^2}\frac{L_c}{1\ {\rm Mpc}}\left(\frac{\Delta L}{1\ {\rm Mpc}}\right)^2. \quad (5)$$

Therefore, we obtain the deflections using (1) and (4) for a distance D; we let the particle propagate an additional ΔD, to see if the particle loses any extra energy. We use the latter approach, looking at extra energy losses, because $\Delta D \ll D$ and does not significantly contribute to the deflection.

Finally, once the particle enters the Galaxy with an arrival energy E, we assign a deflection $\delta_{\rm EG}$ per energy bin of width ΔE via

$$\delta_{\rm EG}(E) = \text{Average}\,\delta_{\rm rms}\ \text{in bin}, \quad (6)$$

where $E \in [E_i, E_i + \Delta E]$. In Fig. 1, we display the values of $\delta_{\rm EG}$ as a function of E. A band $[\delta_{\rm EG} - \omega, \delta_{\rm EG} + \omega]$ is included, such that 68% of the events in the bin is enclosed

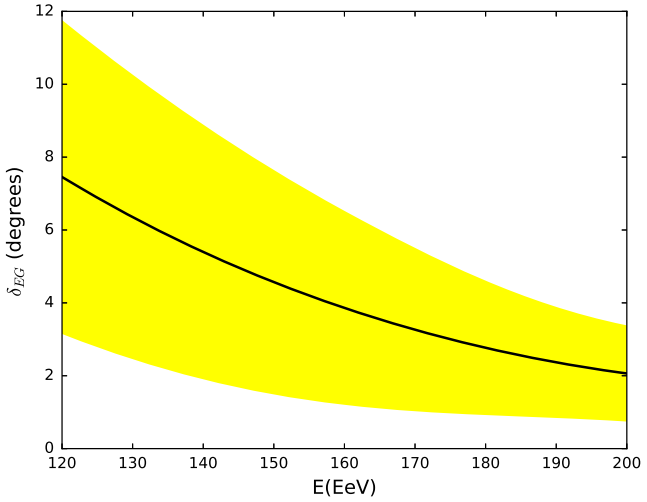

FIG. 1. δ_{EG} as a function of its arrival energy.

in this interval, where we start with deflection intervals ranging between [3°,12°] at 120 EeV until we reach deflection intervals as small as [1°,3°] at 200 EeV.

B. GMF deflections

Once the cosmic ray enters the Galaxy with an energy E, we can ignore energy loss processes due to the relatively small size of the Galaxy ∼40 kpc and trajectory lengths <100 kpc. Thus, the UHECR arrival energy at Earth is also E, and the Galactic magnetic deflections will depend on the rigidity $R = E/(Ze)$.

We use the JF12 GMF model [11,13], which is designed to fit the WMAP7 Galactic synchrotron emission map and more than 40,000 extragalactic Faraday rotation measurements. It is divided into three components: regular (coherent), striated (anisotropic), and an isotropic random field. The latter two are small-scale fields and will be referred to as the random or noncoherent components. We use the best fit values in Ref. [11] for the coherent field parameters and in Ref. [13] for the random field parameters. The small-scale field is assumed to have a coherence length of 60 pc.

We use the backtracking method to determine GMF deflections. For a hypothetical cosmic ray arriving at Earth, we reverse its incoming momentum vector, then change the sign of its charge. We propagate this particle from the Earth, through the GMF, until it leaves the Galaxy. The backtracking is performed using the Runge-Kutta methods in CRPropa3.

We treat the GMF coherent and turbulent components separately, taking advantage of the JF12 field parametrization outlined in Ref. [20]. First, for a given initial direction $P_0 = (l_0, b_0)$ of a UHECR with energy E, where (l, b) are in the Galactic coordinate system with $-180° \leq l < 180°$ the Galactic longitude and $-90° \leq b \leq 90°$ the Galactic latitude, we backtrack it through the coherent field to the position $P_c = (l_c, b_c)$. Starting from P_c, we perform an additional noncoherent field deflection, given by the von Mises-Fisher distribution [21]

$$f(\delta) = \frac{\kappa}{e^{\kappa} - e^{-\kappa}} \exp(\kappa \cos\delta), \tag{7}$$

where $\kappa = \kappa(l_0, b_0, R)$ is a fit parameter and δ is the angular distance between P_c and the final position of the particle. We also assume that the azimuthal distribution of this random deflection is flat. Contrary to the parametrization in Ref. [20], we were forced to extend the Rayleigh distribution to a von Mises-Fisher distribution in order to handle deflections that are not so small. This is caused by the low rigidity particles. The energy dependence in κ is given by

$$\kappa(l_0, b_0, R) = A_1(l_0, b_0)R + A_2(l_0, b_0)R^2. \tag{8}$$

This approximation has been tested in the rigidity range 10 EV $\leq R \leq$ 100 EV. The parameters A_1, A_2 were obtained using HEALPix [22] to divide the sky into 3072 pixels of equal solid angle. We emphasize that in the vicinity of the Galactic plane, where large deflections are present provided by the high turbulent fields components, the parametrization given in Eq. (8) is unreliable and we solve these cases numerically.

In the small deflection hypothesis (valid for <15°), where $\kappa \gg 1$, concentration parameter κ is related to the root-mean-square deflection

$$\delta_{\mathrm{Gal}} = \frac{1}{\sqrt{\kappa}}. \tag{9}$$

We assume an average rigidity $\langle R \rangle_E$ for all particles with a given energy E, which obeys the relation $\langle R \rangle_E \approx (E/10.5\ \mathrm{EeV})\ \mathrm{EV}$ according to our simulations.

Deflections at $R = 10$ EV for different arrival directions are shown in Fig. 2. Coherent deflections are shown in the left panel, and values as large as 90° are observed close to the Galactic center. On the right panel, rms deflections are displayed, where trajectories close to the Galactic center and/or plane can be affected by high (>15°) noncoherent deflections which exceed the angular resolution of experiments (∼2°) by an order of magnitude. As a reference, we have included the reconstructed arrival directions of the high-energy starting event (HESE) neutrino tracks, labeled according to their corresponding event numbers as presented in Ref. [3]. We also marked the respective arrival directions of 10 EV UHECRs, considering the aforementioned tracks as point sources and ignoring EGMFs and the JF12 random field components.

C. Signal and background

We work in a scenario similar to that described in Ref. [5], in which a sample of N_{CR} UHECR and N_ν neutrinos is given. The neutrinos are considered point sources, while the N_{CR} cosmic rays are a combination of

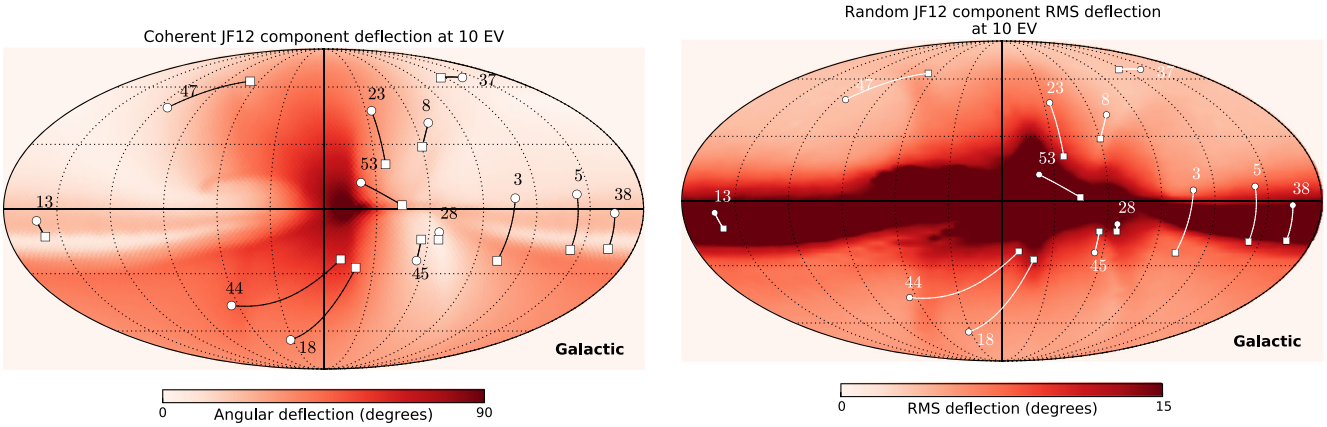

FIG. 2. Left (right) panel: angular (rms) deflections caused by the coherent (random) component of the JF12 field at 10 EV rigidity. The white circles correspond to the reconstructed directions of HESE neutrino tracks, and the white squares mark the expected arrival direction assuming only the JF12 coherent field. The lines joining both are to match UHECRs with their corresponding track; they do not show the actual trajectory taken by the particle. Tracks are labeled by event numbers given in Ref. [3].

signal and background events. We define $\mathcal{S}_i^j$ as the probability density (pdf) that the ith cosmic ray came from the direction of the jth neutrino event,

$$\mathcal{S}_i^j = \frac{\kappa_i}{2\pi(e^{\kappa_i} - e^{-\kappa_i})} \exp(\kappa_i \mathbf{x}_i \cdot \mathbf{x}_j), \tag{10}$$

where $\kappa_i = 1/\sigma_i^2$ and σ_i accounts for the overall smearing of the ith cosmic ray. In the limit of small smearings, $\mathcal{S}_i^j$ reduces to a two-dimensional Gaussian. For single source searches, when $N_\nu = 1$, the signal pdf is $\mathcal{S}_i \equiv \mathcal{S}_i^1$ and is used in the unbinned likelihood analysis like that mentioned in Ref. [23]. For the so-called stacked source searches, when $N_\nu > 1$, we add up the contributions from multiple faint sources, and the signal pdf is modified to

$$\mathcal{S}_i = \frac{1}{N_\nu} \sum_{j=1}^{N_\nu} \mathcal{S}_i^j. \tag{11}$$

To use any of these formulas, we substitute the arrival direction $\mathbf{x}_i$ of the UHECR by its backtracked direction $\mathbf{x}_i'$, assuming that the only magnetic field involved is the regular JF12 component and that the particle's rigidity is given by $\langle R \rangle_E$. We then determine the values of κ_i and $\delta_{\rm Gal}$ via Eq. (8), which parametrizes the smearing effect of the nonregular component, and (9), respectively, which are functions of the UHECR energy and its arrival direction. The EGMF deflections and angular resolution effects are incorporated by making the substitution

$$\kappa_i \to \frac{1}{\sqrt{\delta_{\rm Gal}^2 + \delta_{\rm EG}^2 + \delta_{\rm res}^2}}, \tag{12}$$

with $\delta_{\rm Gal} = \delta_{\rm Gal}(\langle R \rangle_E)$ and $\delta_{\rm EG} = \delta_{\rm EG}(E)$ and where $\delta_{\rm res}$ is the angular resolution of the experiment. We will assume an energy-independent deflection $\delta_{\rm res} = 2°$ as a characteristic angular resolution for IceCube and UHECR ground array experiments.

For the large GMF deflections present at the Galactic plane, where Eq. (8) is not valid, $\mathcal{S}_i$ is determined entirely via Monte Carlo. We also define $\mathcal{B}_i$ as the probability density that the cosmic ray (CR) is a background event.

The background is constructed assuming an isotropic flux of UHECR above 120 EeV outside the Galaxy, following the $E^{-4.5}$ power law measured by TA [5], reaching the Earth nonisotropically due to the GMF deflections. Observed Auger energies are increased by 12% to account for the difference in energy scales between TA and PAO, as explained in Ref. [24].

III. RESULTS

A. Search regions

Now, we quantify how likely it is an observed UHECR, with a given arrival direction $\mathbf{x}_i$ and energy E_i, could have the same origin as the neutrino track, which we treat as the UHECR point source, through the ratio

$$W_i = \frac{\frac{1}{N_\nu} \sum_j \int \mathcal{S}_i^j d\Omega}{\int \mathcal{B}_i d\Omega}, \tag{13}$$

where $d\Omega$ is integrated in a region of 1° in the sky, centered around the neutrino track.

In Fig. 3, we show the effect of W_i in a single point source search, located at IC event 37 $(l, b) = (-137.1°, 65.8°)$ in the northern hemisphere, labeled according to the numbering in Ref. [5], in two plots. One is a two-dimensional map in the coordinates (l, b), where P_c marks the expected UHECR arrival direction, when considering only the JF12 coherent component. The other one is its corresponding one-dimensional projection

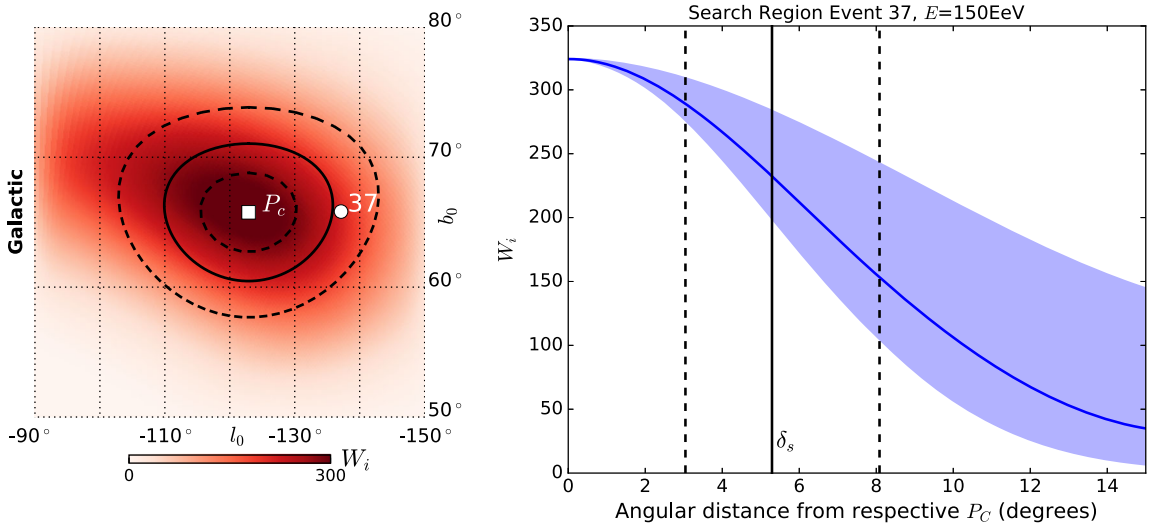

FIG. 3. W_i for a single point source search located at Event 37 and UHECR with energies of 150 EeV. At the left we have the corresponding two-dimensional plot of W_i in the coordinates l_0 and b_0. At the right we have the one-dimensional projection of W_i in the angular distance respect to P_c.

in angular distance centered in P_c, where the solid line is the average value of W_i and the shaded region covers the whole set of values given by the points at the angular distance contour. We have selected IC event 37 because it belongs to a region where the GMF random component deflections are very small, as shown in Fig. 2, being the random EGMF responsible for most of the smearing around P_c, displayed in the two-dimensional plot. These characteristics turn IC event 37 into a candidate for searches of UHECR excesses around it. In both plots, it is clear that P_c gives the highest ratio, since, by construction, it is here where the signal pdf is maximized. Ellipsoidal (vertical) solid/dashed lines are shown for the two- (one-)dimensional plot. The solid line represents the size of the typical or average angular search region $\delta_s = \sqrt{\delta^2_{\rm Gal} + \delta^2_{\rm EG} + \delta^2_{\rm res}}$, measured from P_c, while the dashed lines include the effects of the spread in $\delta_{\rm EG}$ shown in Fig. 1. Our results show that UHECRs confined within the region of size δ_s, which have the appropriate energy and arrival direction, would have very high values of W_i. In the one-dimensional plot, a band enclosing the W_i average is also displayed and is caused by the anisotropy of the random deflections or, equivalently, the B field itself. Otherwise, if the random deflections were isotropic, there would be no band, which means that all the values would converge to a single one. For small angular distances, the variation, or width of the band, of W_i is small because the parameter κ_i is essentially constant, and as we move away from P_c, this variation is significant.

For a wider perspective, we show in Fig. 4 the dependence of δ_s with UHECR arrival energy. It follows the same behavior of $\delta_{\rm EG}$ (see Fig. 1) since δ_s in the case of IC event 37 is dominated by the extragalactic contribution. Based on this energy dependence, in order to avoid dealing with regions extending well over 15°, we impose a minimum energy of 120 EeV.

It is important to mention that in case the current or future ground array experiments are able to identify the UHECR mass we would have a sensible improvement in our analysis since the uncertainties in the rigidity (i.e. $\delta_{\rm EG}$) are going to be small and inside the Galaxy we would know with greater precision the backtrack trajectory because R is constant within the Galaxy. The analysis is also dependent on the UHECR-neutrino sources being within the Greisen-Zatsepin-Kuz'min (GZK) sphere [25,26], such that we may observe the cosmic rays.

The sky map of W_i for a stacked search of cosmic-ray events by using the IceCube tracks as the assumed point

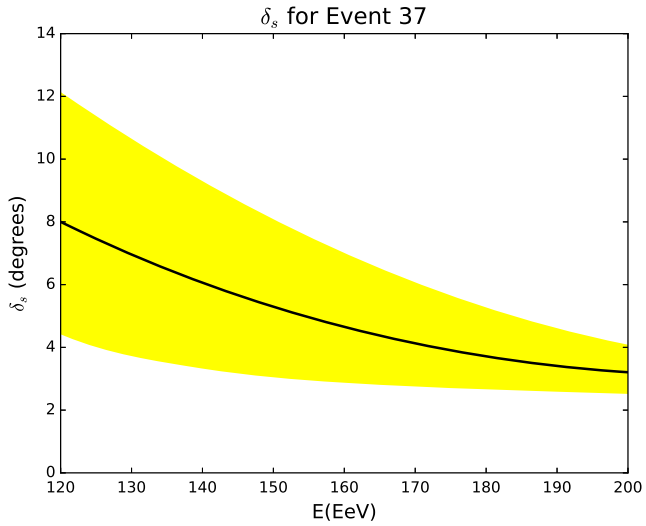

FIG. 4. δ_s angular size region for the IC event 37 as a function of UHECR arrival energy.

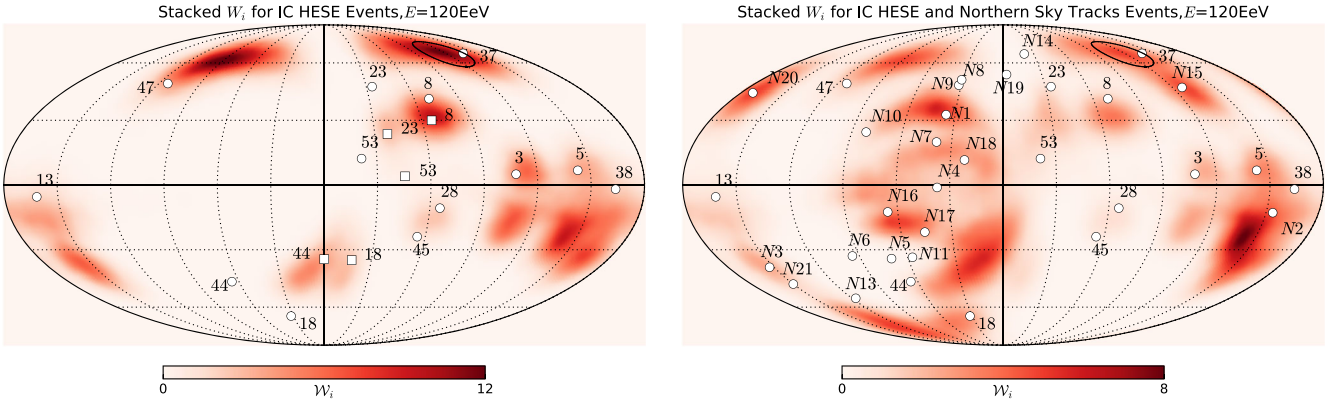

FIG. 5. Sky map for cosmic-ray events of 120 EeV energy and undetermined mass, using the four-year IC HESE events (left panel) and a combined sample of IC HESE events and the two-year IC northern tracks (right panel). The white circles mark the neutrino tracks: HESE tracks are labeled according to their event numbers in Ref. [3]; northern tracks, preceded by the letter N, are numbered according to the order in which they appear in the IceCube Data Release. The white squares mark the respective P_c of the track. Event N12 is not included in the map because it coincides with HESE track 5. The black dashed line marks the equatorial plane. The suggested search region for event 37 is marked with a solid black line.

sources is presented in Fig. 5. Conservatively, we are taking the lower energy bound, which is 120 EeV, for presenting our results in this figure.

This figure contains two sky maps, one for the IC HESE event sample [5] and the second one using both the four-year HESE tracks and the two-year IceCube Northern sky tracks [16] in a combined search. As before, the circles represent the positions of the neutrino tracks. In the HESE sky map, we also included squares indicating their respective points P_c when the neutrino tracks are close to each other. Here, we observe that for events close to the Galactic plane we do not have a well-defined region to correlate with the neutrino track. Instead, we have disjoint regions, above and below the Galactic plane, which represent similar low values of W_i, such as those in neutrino events 3, 5 and 38. This is caused by the large random component deflections in these regions, as we have seen in Fig. 2. There are out-of-plane events, such as events 8 and 23, 18 and 44, 28 and 45, which exhibit well-defined regions, but with the drawback that they may overlap with each other. Despite our inability to disentangle the point source of origin, these zones are interesting to look for UHECR excesses, because the effect of GMF deflections is significantly reduced and obtains higher values of W_i. The ideal cases for correlating UHECRs with these neutrino tracks are the events 37 and 47, which are far away from the Galactic plane.

In the combined sky map, we increase the number of regions where we can expect the arrival of UHECRs. However, due to the nature of the stacked search, which includes a $1/N_\nu$ factor in Eq. (11), the W_i of well-spread tracks is flattened to very low values (see, for example, events 8 and 47). Meanwhile, when we have clustered tracks, the W_i are strongly enhanced, as we can see in the region close to $(l, b) = (0°, -30°)$. Even when using the enlarged sample, the suggested search region for HESE event 37 does not overlap with the others. It is interesting to highlight that the northern event $N2$ exhibits a region with very large values of W_i, which is enhanced by contributions from events 3 and 38 and the low values of the background pdf in the area.

B. Stacked search with the current experimental data

We have translated our stacked search expectations of UHECR arrival directions, obtained from combining the HESE and northern tracks information, into a joint data likelihood analysis using TA and PAO. Only the 12 UHECR events above 120 EeV (after scaling Auger energies as mentioned in Sec. II C) are considered in this analysis. For this search, we have included detector effects and assumed an energy spectrum for the signal. This is achieved by using a modified map defined by

$$\mathcal{S}_i^{\mathrm{mod}} = \frac{\tilde{\mathcal{S}}_i \omega(\delta_i)}{\int \tilde{\mathcal{S}}_i \omega(\delta) d\Omega}, \tag{14}$$

where $\tilde{\mathcal{S}}_i$ is the convolution of the sky maps with the energy spectrum $\Phi(E)$

$$\tilde{\mathcal{S}}_i = \frac{\int \mathcal{S}_i(E)\Phi(E)dE}{\int \Phi(E)dE}. \tag{15}$$

Here, S_i is given by Eq. (11). We will assume that the signal has the same energy spectrum as the background $\Phi(E) = E^{-4.5}$ and that the energy integrals are evaluated above 120 EeV. The function $\omega(\delta)$ is the combined exposure of the experiments, and δ_i is the declination at $\mathbf{x}_i$. The exposure ω is defined as

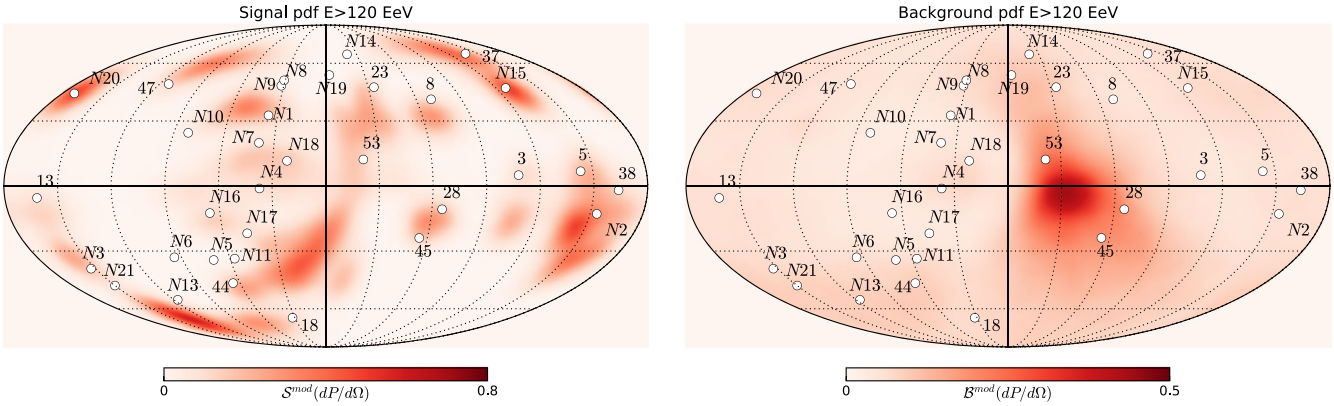

FIG. 6. Signal and background pdfs used for the likelihood analysis in Sec. III B, to be inserted directly into Eq. (17).

$$\omega(\delta) = \frac{N_{\rm TA}\omega_{\rm TA}(\delta) + N_{\rm PAO}\omega_{\rm PAO}(\delta)}{N_{\rm TA} + N_{\rm PAO}}. \tag{16}$$

$N_{\rm TA}$ and $N_{\rm PAO}$ are the number of cosmic rays above 120 EeV detected by each experiment, and $\omega_{\rm TA}$ and $\omega_{\rm PAO}$ are their respective normalized exposures, extracted from the plots in Ref. [5]. This lets us obtain a sky map that only depends on the UHECR arrival direction $\mathbf{x}_i$. The same prescription is used to obtain a modified background map $\mathcal{B}_i^{\rm mod}$.

The sky maps obtained from Eq. (14) are shown in Fig. 6. The hot spot seen on this new background pdf distribution is a feature of the incoming flux; it is only mildly affected by the exposure and different options of power law spectral indices within the uncertainties reported by TA.

Our statistical analysis relies on the likelihood formula

$$\mathcal{L}(n_s) = \prod_{i=1}^{N_{\rm CR}} \left[\frac{n_s}{N_{\rm CR}}\mathcal{S}_i^{\rm mod} + \left(1 - \frac{n_s}{N_{\rm CR}}\right)\mathcal{B}_i^{\rm mod}\right], \tag{17}$$

where n_s is a fit parameter and $N_{\rm CR} = 12$, and we define the test statistic

$$\lambda = 2\ln\left[\frac{\mathcal{L}(\hat{n}_s)}{\mathcal{L}(0)}\right], \tag{18}$$

where $\hat{n}_s$ is the best-fit value that maximizes the likelihood. We obtain a value $\lambda = 0.65$ which, when compared to the background-only test statistic distribution, yields a p value of 0.20, consistent with the results presented in Ref. [5] that correspond to nonsignificant excesses.

C. Future prospects

With the aim of providing future predictions, we consider a second scenario in which we estimate the necessary exposure time to find correlations between the HESE and northern tracks with the TA UHECR arrival directions alone. For this purpose, we estimate the expected number of signal events n_s^{90} as the 90% C.L. sensitivity using only TA data. n_s^{90} is defined as the mean number of injected signal events required to obtain a p value below 0.5 on 90% of the trials. This value is proportional to the current live time T_0 and the point source flux Φ_s of each individual source. Considering that the expected number of signal and background events increases linearly in time, we can obtain the time T' required to achieve a 5σ discovery given the current sensitivity. This is defined by the relation

$$\frac{T'}{T_0} n_s^{90} = n_s^{5\sigma}(T'), \tag{19}$$

where $n_s^{5\sigma}$ is defined as the mean number of injected events required to obtain a p value corresponding to more than 5σ on 50% of the trials. These definitions of sensitivity and discovery potential have also been used in Ref. [5].

The current expected number of background events is taken to be 7 so that it matches the TA data. Now, if we consider the current experimental capacity of TA, it would require a live time of 72 years to satisfy this condition, amounting to slightly over ten times its current live time of 7 years. Certainly, these results can be improved with the new upgrade to PAO, which should provide further information on the mass composition and the energy flux at the highest energies [27]. The ability to estimate the mass of incoming particles on a shower-by-shower basis allows us to select the lightest particles to obtain smaller, sharper search regions that the ones presented in Fig. 5.

IV. SUMMARY AND CONCLUSIONS

We have built two sky maps showing different regions where UHECR excesses with respect to the isotropic background should appear at an energy of 120 EeV: one for the IC four-year HESE tracks and another for a combined search using the four-year HESE events and the two-year Northern sky tracks. These excesses are inferred from the measurement of the correlation between a given UHECR arrival direction with the IceCube neutrino

tracks, which are taken as point sources. The GMF and EGMF deflections have been calculated, using, correspondingly, the JF12 model and EGMF of strength ~ 1 nG and coherence lengths $\gtrsim 1$ Mpc. We note that the out-of-plane regions concentrate higher correlation values, quantified by the probability ratio W_i, being more promising than the ones near the Galactic plane for revealing excesses. Some of these regions can be correlated clearly with a single neutrino track, for instance, in events 37 and 47. These events are candidates to include in a point source search. For the stacked source search, good candidates include the tracks that contribute to the region in $(l, b) = (0°, -30°)$ and $(l, b) = (-150°, -30°)$.

In particular, we take a closer look into event 37, where the GMF random component is negligible, considering an energy of 150 EeV and getting a region, where most of the UHECR excess should be located, of angular size $\sim 5°$. If the UHECRs had energies of 120 or 200 EeV, the angular size would be $\sim 8°$ or $\sim 3°$, respectively. This similar tendency can be extrapolated to the sky map where we expect regions with a much smaller angular spread, as long as we increase the UHECR energy. Naturally, the possibility to find UHECR in these regions intrinsically depends on these sources being located within the GZK sphere.

Finally, we have not found correlations when we put our stacked search approach in terms of a statistical analysis based on TA and PAO data. We also obtained a projected live time of 72 years for TA to find some correlations. Clearly, this result should improve once the PAO upgrade is operational, allowing us to determine mass composition in a shower-by-shower basis and select the lightest events, giving as a consequence narrower signal pdfs.

ACKNOWLEDGMENTS

The authors gratefully acknowledge DGI-PUCP for financial support under Grant No. 2014-0064 as well as CONCYTEC for a graduate fellowship under Grant No. 012-2013-FONDECYT. The authors also want to thank Mauricio Bustamante and José Bellido for useful suggestions.

[1] M. G. Aartsen *et al.* (IceCube Collaboration), Science **342**, 1242856 (2013).
[2] M. G. Aartsen *et al.* (IceCube Collaboration), Phys. Rev. Lett. **113**, 101101 (2014).
[3] M. G. Aartsen *et al.* (IceCube Collaboration), *Proc. Sci.*, ICRC2015 (2015) 1081.
[4] R. Aloisio, arXiv:1603.05886.
[5] M. G. Aartsen *et al.* (IceCube, Pierre Auger, and Telescope Array Collaborations), J. Cosmol. Astropart. Phys. 01 (2016) 037.
[6] M. Santander *et al.* (VERITAS and IceCube Collaborations), *Proc. Sci.*, ICRC2015 (2015) 785.
[7] M. G. Aartsen *et al.* (IceCube and LIGO-Virgo Collaborations), Phys. Rev. D **90**, 102002 (2014).
[8] M. W. E. Smith *et al.*, Astropart. Phys. **45**, 56 (2013).
[9] K. Dolag, D. Grasso, V. Springel, and I. Tkachev, JETP Lett. **79**, 583 (2004).
[10] G. Sigl, F. Miniati, and T. A. Enßlin, Phys. Rev. D **70**, 043007 (2004).
[11] R. Jansson and G. R. Farrar, Astrophys. J. **757**, 14 (2012).
[12] M. S. Pshirkov, P. G. Tinyakov, P. P. Kronberg, and K. J. Newton-McGee, Astrophys. J. **738**, 192 (2011).
[13] R. Jansson and G. R. Farrar, Astrophys. J. **761**, L11 (2012).
[14] A. Porcelli *et al.* (Pierre Auger Collaboration), *Proc. Sci.*, ICRC2015 (2015) 420.
[15] A. Aab *et al.* (Pierre Auger Collaboration), Phys. Rev. D **90**, 122005 (2014).
[16] M. G. Aartsen *et al.* (IceCube Collaboration), Phys. Rev. Lett. **115**, 081102 (2015).
[17] R. Alves Batista *et al.*, Eur. Phys. J. Web Conf. **99**, 13004 (2015).
[18] R. C. Gilmore, R. S. Somerville, J. R. Primack, and A. Domínguez, Mon. Not. R. Astron. Soc. **422**, 3189 (2012).
[19] S. Mollerach and E. Roulet, J. Cosmol. Astropart. Phys. 10 (2013) 013.
[20] J. A. Carpio and A. M. Gago, Phys. Rev. D **93**, 023004 (2016).
[21] R. Fisher, Proc. R. Soc. A **217**, 295 (1953).
[22] K. M. Gorski, E. Hivon, A. J. Banday, B. D. Wandelt, F. K. Hansen, M. Reinecke, and M. Bartelmann, Astrophys. J. **622**, 759 (2005).
[23] J. Braun, J. Dumm, F. De Palma, C. Finley, A. Karle, and T. Montaruli, Astropart. Phys. **29**, 299 (2008).
[24] R. Abbasi *et al.* (Pierre Auger and Telescope Array Collaborations), J. Phys. Soc. Jpn. Conf. Proc. **9**, 010016 (2016).
[25] K. Greisen, Phys. Rev. Lett. **16**, 748 (1966).
[26] G. T. Zatsepin and V. A. Kuz'min, JETP Lett. **4**, 78 (1966).
[27] A. Aab *et al.* (Pierre Auger Collaboration), arXiv:1604.03637.